RL-TR-92-99
In-House Report
April 1992

EFFECTS OF SPATIAL LIGHT MODULATOR TRANSMISSIVE AND REFLECTIVE DEAD ZONES ON OPTICAL CORRELATION

Peter D. Gianino, Charles Woods

APPROVED FOR PUBLIC RELEASE; DISTRIBUTION UNLIMITED

Rome Laboratory
Air Force Systems Command
Griffiss Air Force Base, NY 13441-5700

This report has been reviewed by the Rome Laboratory Public Affairs Office (PA) and is releasable to the National Technical Information Service (NTIS). At NTIS it will be releasable to the general public, including foreign nations.

RL-TR-92-99 has been reviewed and is approved for publication.

APPROVED: Richard Payne

RICHARD PAYNE, Chief
Photonic Devices Technology Division

FOR THE COMMANDER: Harold Roth

HAROLD ROTH, Director
Electromagnetics & Reliability Directorate

If your address has changed or if you wish to be removed from the Rome Laboratory mailing list, or if the addressee is no longer employed by your organization, please notify RL(ERO) Hanscom AFB MA 01731-5000. This will assist us in maintaining a current mailing list.

Do not return copies of this report unless contractual obligations or notices on a specific document require that it be returned.

REPORT DOCUMENTATION PAGE

Form Approved
OMB No. 0704-0188

1. AGENCY USE ONLY (Leave blank)	2. REPORT DATE	3. REPORT TYPE AND DATES COVERED
	April 1992	Scientific, Interim

4. TITLE AND SUBTITLE

Effects of Spatial Light Modulator Transmissive and Reflective Dead Zones on Optical Correlation

5. FUNDING NUMBERS

PE: 61102F
PR: 2305
TA: J7
WU: 11

6. AUTHOR(S)

Peter Gianino
Charles Woods

7. PERFORMING ORGANIZATION NAME(S) AND ADDRESS(ES)

Rome Laboratory/ERO
Hanscom AFB, MA 01731-5000

8. PERFORMING ORGANIZATION REPORT NUMBER

RL-TR-92-99

9. SPONSORING/MONITORING AGENCY NAME(S) AND ADDRESS(ES)

10. SPONSORING/MONITORING AGENCY REPORT NUMBER

11. SUPPLEMENTARY NOTES

12a. DISTRIBUTION/AVAILABILITY STATEMENT

Approved for public release; distribution unlimited

12b. DISTRIBUTION CODE

13. ABSTRACT (Maximum 200 words)

We present both analytical calculations and computer simulations for optical correlation in correlators using pixellated Spatial Light Modulators (SLM) with transmissive (or reflective) dead zones. The input plane SLM modulates the intensity in its active areas while its dead zones transmit (or reflect) all of the light. In the filter plane SLM the dead zones are similar, but the active areas modulate both phase and transmittance to produce either a phase-only filter, a binary phase-only filter, or a classical matched filter. When these dead zones appear in the input plane, we add a dc block in the filter plane for noise reduction and use a filter reference image that is smaller than the input SLM size to reduce false correction peaks. We calculate the correlation peak intensity, the signal-to-noise ratio and the energy throughput efficiency as a function of dead zone area in both the input and filter plane SLMs. Analysis shows that the opaque dead zone results are a special case of the transmissive dead zone results. We also calculate peak intensities when one SLM has opaque dead zone and the other, transparent dead zone.

14. SUBJECT TERMS	15. NUMBER OF PAGES
Dead zones; Optical correlator; Phase-only filter; Spatial light modulator	44
	16. PRICE CODE

17. SECURITY CLASSIFICATION OF REPORT	18. SECURITY CLASSIFICATION OF THIS PAGE	19. SECURITY CLASSIFICATION OF ABSTRACT	20. LIMITATION OF ABSTRACT
UNCLASSIFIED	UNCLASSIFIED	UNCLASSIFIED	SAR

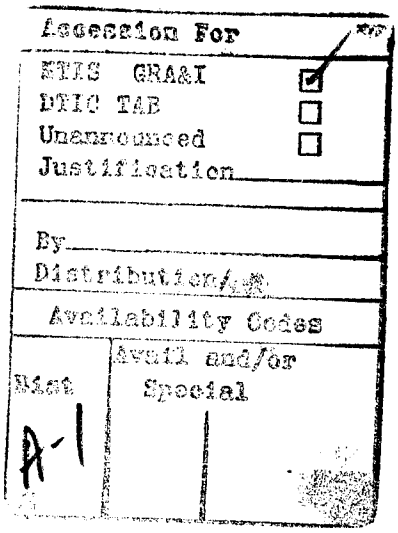

Contents

Illustrations

Tables

Acknowledgement

We express our appreciation to Dr. Joseph Horner of Rome Laboratory, Hanscom Air Force Base, for invaluable discussions and suggestions.

Effects of Spatial Light Modulator Transmissive and Reflective Dead Zones on Optical Correlation

1. INTRODUCTION

We previously analyzed the effects of opaque dead zones (ODZs) in pixels of spatial light modulators (SLMs) used in standard 4-f or 2-f optical correlators.[1] There, we showed by computer simulation and approximate analytical calculations how changes in these ODZs affected the correlator's signal-to-noise ratio, correlation peak intensity, and the efficiency of the system's light throughput when either a phase-only filter (POF), a binary phase-only filter (BPOF), or a classical matched filter (CMF) is used in the filter plane.

Our goal here is to examine how these same correlator performance characteristics are affected when pixels in the dead zone portions of the SLM, rather than completely blocking the incident light, completely transmit (or reflect) it towards the output detector. Since the mathematics describing the reflecting mode is identical to that describing the transmitting mode, we will refer to both of them as transmissive dead zone (TDZ). In this report we provide accurate analytical calculations and additional simulations for TDZ using the same three filters as above. We will also show that the analytical treatment of TDZ is a general one because it includes the ODZ, as well as the mixture of ODZ and TDZ, as special cases.

Received for Publication 13 April 1992

1 Gianino, P.D. and Woods, C.L. (1992) Effects of spatial light modulator opaque dead zones on optical correlation, *Appl. Opt.*, **31**:4025-4033.

Furthermore, we allow for the possibility of placing a dc block at the center of the filter plane SLM. For the simulation we follow the same sequence of computer operations shown in the computer flow diagram in Figure 2 of Reference 1.

2. BACKGROUND

The SLMs in the input and filter planes, designated as SLM1 and SLM2, respectively, and the detector in the output plane are assumed to have arrays of 64x64 pixels. We adopt the model that each pixel of a SLM is subdivided into two regions. One region, called the "active zone" (AZ), encodes the addressed amplitude or phase signal modulating any light incident on it. The remaining region of the pixel, called the "dead zone" (DZ), does not encode any of the addressed amplitude or phase signal. In our model this dead zone is either opaque (blocking 100 percent of any light incident upon it), or transparent (transmitting or reflecting all of this light). Examples of SLMs whose dead zones are opaque are SEED, symmetric SEED, magneto-optic, Fabry-Perot etalon and PLZT devices. Liquid crystal TVs have transmissive DZs, while the deformable mirror devices have reflective DZs. Other devices, such as liquid crystal light valves, microchannel SLMs and ferroelectric liquid crystal SLMs, have more complicated DZs, but these could be approximately modeled by assuming an average value of the complex amplitude transmittance.

3. MATHEMATICAL ANALYSIS

3.1 Input Plane

A diagram of a typical pixel in SLM1 is shown in Figure 1; x_1, y_1, are the spatial coordinates in the input plane. The AZ (the light area) is positioned at the center, while the transmissive (or reflective) DZ (the dark area) is located around the edge. The dimensions of the pixel are given by c_x, c_y; those of the AZ by b_x, b_y. A similar diagram describes the typical pixel in the filter plane, except that the dimensions of the pixel are given by h_x, h_y and those of its AZ by e_x, e_y. The fractional areas for the dead zones in both SLMs are specified as

$$Z_1 = 1 - b_x b_y / c_x c_y \quad \text{(for SLM1)} \tag{1}$$

$$Z_2 = 1 - e_x e_y / h_x h_y \quad \text{(for SLM2)} \tag{2}$$

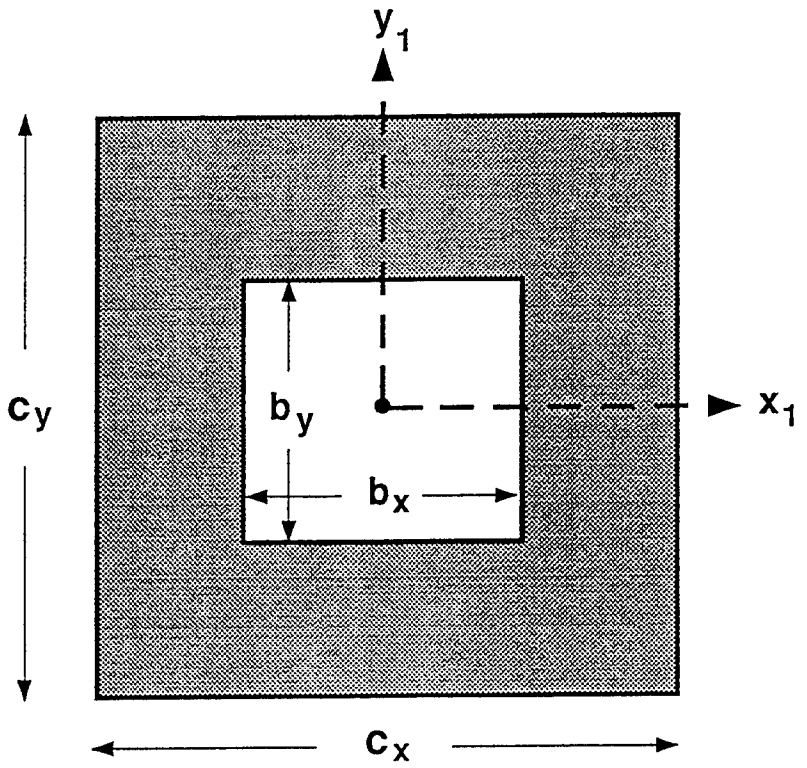

Figure 1. Diagram of a Typical Pixel of Dimensions c_x, c_y in SLM1. The active zone in the center has dimensions b_x, b_y. The darkened area corresponds to the transmissive (or reflective) dead zone.

The spatial coordinates in the filter plane are given by x_2, y_2, while the spatial frequency coordinates in that same plane are given by ξ_2, η_2.

A block diagram depicting the various system components and signals involved in the correlation process is shown in Figure 2; $s(x_1, y_1)$ is a continuous input signal. The final signal amplitude encoded on SLM1 due to the active areas in the pixels is the function $w(x_1, y_1)$. According to our model, this function is constant within a given active zone (the constant value representing a sampled version of s) and is zero in the DZ (a detailed mathematical description of w and the other functions to be introduced will be given in the Appendix). The DZ of each pixel in SLM1 transmits (or reflects) 100 percent of the light illuminating it. This light from the DZ transmittance is represented by $t_s(x_1, y_1)$. The sum of the exiting signals w and t_s are Fourier transformed (FT) by lens 1 into the sum of transforms $W(\xi_2, \eta_2)$ and $T_s(\xi_2, \eta_2)$ respectively, where (ξ_2, η_2) are spatial frequency coordinates in the filter plane.

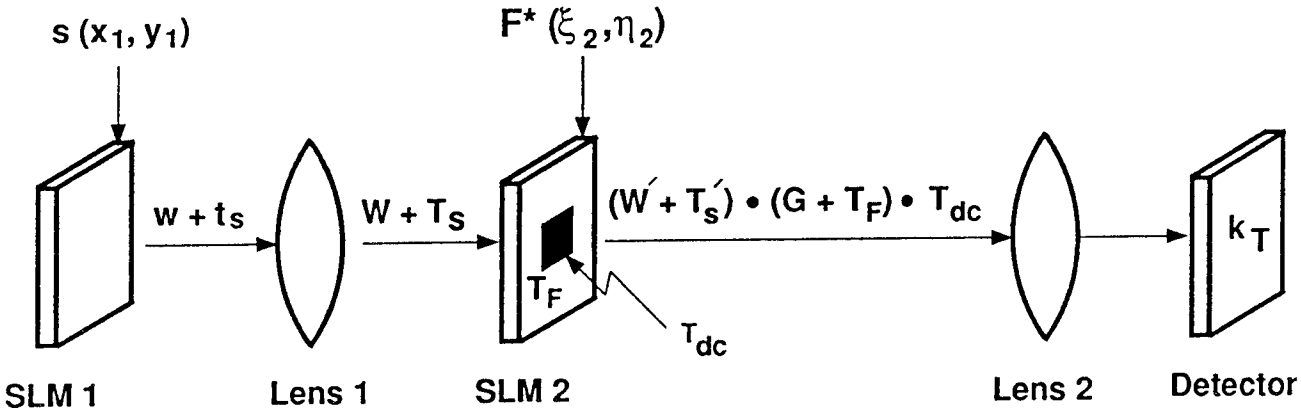

Figure 2. Block Diagram of Correlator Showing the Different Components and Signals Involved in the Correlation Process. The various signals are explained in the text.

3.2 Filter Plane

The function $F^*(\xi_2, \eta_2)$ is the continuous filter transform function for one of the three desired filters. The final amplitude of the filter transform function encoded on SLM2 due to the active areas in the pixels is the function $G(\xi_2, \eta_2)$. According to our model, this function is constant within a given AZ (the constant value representing a sampled version of F^*) and is zero in the DZ. Analytically, F^* is formed from the Fourier transform of $s(x_1, y_1)$ and G is obtained from F^* (see Eq. (A-12) in the Appendix).

The DZ of each pixel in SLM2 not only reduces the optical efficiency of the filter, but it also introduces noise by transmitting (or reflecting) all of the incident light. This unwanted DZ transmittance is designated by $T_F(\xi_2, \eta_2)$. Furthermore, a transmissive dead zone in a SLM acts like a grating, transmitting a significant part of its energy into the (0, 0) order and diffracting the rest into higher order images. The physical size of SLM2 is chosen so as to transmit only the (0, 0) orders of W and T_s onto SLM2. These transmitted portions are designated by W' and T_s', respectively. The remaining diffraction orders fall outside of the SLM and are blocked. Since the T_s' portion contributes noise and is localized around the optic axis, an opaque dc block (at the (0, 0) frequency position) eliminates a great deal of this input TDZ noise from the system. This dc block, whose transmittance is given by $T_{dc}(\xi_2, \eta_2)$, is indicated by the small dark rectangle at the center of SLM2 in Figure 2. The net signal exiting from SLM2 consists of four product terms: a signal term $W'.G.T_{dc}$, two imaged noise terms $(W'+T_s').T_F.T_{dc}$, and a filtered noise term $T_s'.G.T_{dc}$. The resulting four terms are transformed by lens 2 to produce a total correlation amplitude pattern $k_T(x_3, y_3)$ at the detector, where x_3, y_3 are spatial coordinates in the detector (or output) plane.

3.3 Output Plane

The total correlation amplitude k_T can be written as the sum of the inverse Fourier transforms of the four product terms mentioned above. These four terms may be written explicitly as

$$k_c(x_3, y_3) \equiv FT^{-1}\{W'.G.T_{dc}\} = [w'(x_3, y_3) * g(x_3, y_3)] \odot t_{dc}(x_3, y_3) \tag{3}$$

$$k_s(x_3, y_3) \equiv FT^{-1}\{W'.T_F.T_{dc}\} = [w'(x_3, y_3) \odot t_F(x_3, y_3)] \odot t_{dc}(x_3, y_3) \tag{4}$$

$$k_R(x_3, y_3) \equiv FT^{-1}\{T_s'.T_F.T_{dc}\} = [t_s'(x_3, y_3) \odot t_F(x_3, y_3)] \odot t_{dc}(x_3, y_3) \tag{5}$$

$$k_{FR}(x_3, y_3) \equiv FT^{-1}\{T_s'.G.T_{dc}\} = [t_s'(x_3, y_3) * g(x_3, y_3)] \odot t_{dc}(x_3, y_3) \tag{6}$$

where FT^{-1} refers to the inverse Fourier transform operation, $*$ represents the correlation operation, $\odot$ the convolution operation and w', t_s', g, t_F and t_{dc} are the inverse Fourier transforms of W', T_s', G, T_F and T_{dc}, respectively. Equations (3) and (6) contain the correlation operation because of the complex conjugate term in the g function.

For these and subsequent equations we employ the following notation for certain functions that occur repeatedly in both the input and detector planes:

$$v_x \equiv \text{rect}(x/b_x)/b_x \tag{7}$$

$$q_x \equiv \text{sinc}(x/c_x)/c_x \tag{8}$$

$$m_x \equiv \text{sinc}(e_x x/h_x L_x) \tag{9}$$

$$r_x \equiv \text{rect}(x/L_x) \tag{10}$$

in which

$$\mathrm{sinc}(\alpha) \equiv (\sin\pi\alpha)/\pi\alpha. \tag{11a}$$

and

$$\mathrm{rect}\left(\frac{x}{x_0}\right) \equiv \begin{cases} 0, |x| > x_0 \\ 1, |x| < x_0 \end{cases} \tag{11b}$$

We also utilize the fact that $q_i \odot q_i = q_i$ for i=x or y. L_x is the x dimension length of SLM1 as well as of the detector, and the variable x can refer to either x_1 or x_3, depending upon which plane is being referred to. There will be another set, namely, v_y, q_y, m_y, and r_y, which have the same functional forms as above, with all x subscripts and variables replaced by y. In the limit of small pixel and active zone sizes (that is, b, c, e, h<<L and e<<h), functions v and q of Eqs. (7) and (8) become δ functions, and functions m and r of Eqs. (9) and (10) become flat over the SLM faces.

The explicit 2D forms for the functions w', t_s', g, t_F, and t_{dc}, which are mentioned in Eqs. (3)-(6), as well as their Fourier transforms, are derived in the Appendix. Their final forms are given in Eqs. (A-7), (11), (13), (17), and (20), respectively. When these are substituted into Eqs. (3)-(6) and only the zero diffraction order terms are kept, there results

$$k_c(x_3, y_3) = (1-Z_1)\,(1-Z_2) \tag{12}$$

$$\left\{\left[\left(s(x_3, y_3) \odot v_x v_y\right) \cdot r_x r_y\right] * \left[f^*(-x_3, -y_3) \cdot m_x m_y\right] \odot q_x q_y\right\} \odot t_{dc}$$

$$k_s(x_3, y_3) = (1-Z_1)\, Z_2 \left\{\left[\left(s(x_3, y_3) \odot v_x v_y\right) \cdot r_x r_y\right] \odot q_x q_y\right\} \odot t_{dc} \tag{13}$$

$$\equiv Z_2 \cdot w'(x_3, y_3) \odot t_{dc}$$

$$k_R(x_3, y_3) = Z_1 Z_2 \left[r_x r_y \odot q_x q_y\right] \odot t_{dc} \equiv Z_2 \cdot t_s'(x_3, x_3) \odot t_{dc} \tag{14}$$

$$k_{FR}(x_3, y_3) = Z_1(1-Z_2) \left\{\left(r_x r_y * \left[f^*(-x_3, -y_3) \cdot m_x m_y\right]\right) \odot q_x q_y\right\} \odot t_{dc} \tag{15}$$

The inverse Fourier transform of F^*, denoted by f^*, is also known as the impulse response of F^* or the filter reference image.

These equations reveal the basic operation of the system. They clearly show that the final correlation consists of a "true" correlation term (the one containing $s*f^*$), plus three background terms. The true correlation term, k_c of Eq. (12), is produced solely from the active zones in the input and filter SLMs. It is identical to the ODZ correlation discussed in Reference 1 and given specifically by Eq. (6) there. Under these conditions, Eqs. (4)-(6) and, therefore, Eqs. (13)-(15), vanish because $t_s(x_1, y_1)=T_F(\xi_2, \eta_2)=0$. The three remaining k terms in Eqs. (13)-(15) contribute to the background noise and coherently interfere with the k_c signal term. For example, the "signal" image background term k_s is the image of the input signal that has passed through the DZ area of the filter SLM. The appearance of input images in the output plane has been noted by Goodman[2] for the Vander Lugt correlator and by Flavin and Horner[3] for the amplitude-encoded phase-only filter. Neither of these cases, however, exhibit the specific TDZ behavior considered here. The "rectangular input TDZ " background term k_R is the image of the rectangular-shaped TDZof the input SLM that has also passed through the TDZ area of the filter SLM. The "filtered rectangular input TDZ " background term k_{FR} is the light from the TDZ of all pixels in the input SLM that has passed through the filter's AZ areas. The energy of this light is concentrated near the on-axis pixels of the filter, producing a slowly varying pattern in the correlation plane. As indicated in the above equations, these three noise terms are proportional to a product of a TDZ and either an AZ or a TDZ.

Because of the pixellation of the SLMs, all 4 terms have replicated images, with their (0, 0) order on axis and weaker orders off axis. For example, k_R is a series of 2D rect functions in the output plane, with the central one being the highest and the others diminishing in height as they get farther away from the center. The k_s, k_R, and k_{FR} terms coherently interfere with and increase the correlation peak and may also contribute secondary maxima. Such higher order peaks were detected in computer simulations by Yu[4] and in experiments by Javidi.[5] In addition, both have been detected in experiments and analyzed mathematically by Davis, et al.[6] All of these investigations involved systems that employed a binarized version of the joint transform correlator (JTC). With a dc block, k_s, k_R, and k_{FR} are high-pass filtered (or edge-enhanced), thus decreasing the noise.

---

2 Goodman, J.W. (1968) *Introduction to Fourier Optics*, McGraw-Hill Book Co., NY, Chap. 7, pp. 174-177.

3 Flavin, M.A. and Horner, J.L. (1989) Amplitude encoded phase-only filters, *Appl. Opt.*, **28**:1692-1696.

4 Yu, F.T.S., Cheng, F., Nagata, T. and Gregory, D.A. (1989) Effects of fringe binarization of multiobject joint transform correlation, *Appl. Opt.*, **28**:2988-2990.

5 Javidi, B. and Horner, J.L. (1989) Multifunction nonlinear signal processor: deconvolution and correlation, *Opt. Eng.*, **28**(8):837-843.

6 Davis, J.A., Merrill, E.A., Cottrell, D.M. and Bunch, R.M. (1990) Effects of sampling and binarization in the output of the joint Fourier transform correlator, *Opt. Eng.*, **29**(9):1094-1100.

In the Appendix we show that the functions appearing in the filter plane are limited by the finite size of SLM2 and are, therefore, low-pass filtered in this plane. This low-pass filtering produces the q terms in Eqs. (12)-(15). Note that the filter reference image position changes the correlation peak, as described in Eq. (12), by the factors $m_x m_y$. The qualitative results that can be gleaned from Eqs. (12)-(15) are analyzed more fully in Section 5.

4. COMPUTER SIMULATIONS

For computational purposes each SLM pixel is simulated by sampling at 16 points, arranged in a square array having 4 points on a side. Of these 16 points a certain fraction Z_i is considered to make up the dead zone (DZ) area of SLM_i, and the remaining fraction $(1-Z_i)$ is considered to make up the (AZ) area of SLM_i. The 4x4 point sampling of the 64x64 pixels in both input and filter planes produces arrays of 256x256 points. To simultaneously produce this resolution in both planes, additional zeroes must be added to bring the final arrays to 1024x1024 points.[1]

The computer simulations used the same input signal as in Reference 1 (namely, a girl's face) with each of the three filters. The quantities computed from the resulting correlation pattern were its peak intensity value and its signal-to-noise ratio (SNR). The percentages of the energy incident on or lost at the three different planes of the system were also evaluated. Three different cases involving TDZ were studied and are listed in Table 1: Case A, in which both SLMs have equal amounts of DZ; Case B, in which only SLM1 has DZ; and Case C, in which only SLM2 has DZ. These cases are the same as in Reference 1 except that in this study the number of sampling points per pixel are always fixed at 4 on a side ($N_1=N_2=4$).

Table 1. TDZ Cases Studied

CASE	SLM1	SLM2	NON-ZERO k TERMS IN k_T
A	Z_1 varies	$Z_2 = Z_1$	k_c, k_s, k_R, k_{FR}
B	Z_1 varies	$Z_2 = 0$	k_c, k_{FR}
C	$Z_1 = 0$	Z_2 varies	k_c, k_s
If $Z_1 = Z_2 = 0$ for any case			k_c

It should be mentioned that other investigators[7,8,9] have set up mathematical models to compute how pixellation and dead zones in real SLMs such as deformable mirror devices and magneto-optic SLMs affect correlation. Their systems were of both the 4f and Joint Transform Correlator types. In each case, however, their computer simulations[7,8,9] and experiments[9] were limited to that one particular configuration of DZ peculiar to each type of SLM and presented no careful analytical correlation calculations. No investigations have studied the effects due to changes in DZ.

4.1 Correlation Peak Intensity

Figure 3 shows how the computer-calculated normalized correlation peak intensity $I_p(=k_T^2)$ changes with equal input and filter TDZ for Case A using each of the three filters. The abscissa Z_i refers to the TDZ in both SLMs since $Z_1=Z_2=Z_i$ for Case A. These intensities are normalized to that value, namely (I_p=8.31) for the POF when $Z_1=Z_2=0$ and no dc block is inserted in the filter plane.

The solid lines in Figure 3 give the I_p for the ODZ condition without a dc block. These are the same as the three solid curves in Figure 6 of Reference 1 and are repeated here for reference. A dc block is not required for ODZ since no noise is present. The dashed lines give the I_p for the TDZ condition with a 1-pixel dc block placed at the center of SLM2. The dashed lines are generally higher than the solid lines because the additional light getting through the transparent dead zones increases I_p. For Z_i=0 the dc block significantly decreases only the CMF correlation peak. For both of the phase filters the dotted and solid lines are fairly close up to DZs of about 20 percent. Just as in the opaque condition, the I_p decrease as TDZ increases. However, at some point the I_p go through a minimum and begin to increase. This occurs at DZs of about 20 percent for the CMF and about 75 percent for both of the phase filters. This happens because large amounts of light (which is really noise) from the TDZs are added to the correlation pattern. Finally, when TDZ reaches 100 percent, all three dashed curves come together at a normalized intensity of 0.07. This seems reasonable because at 100 percent TDZ both SLMs are completely transparent: transmitting all of the incident light (represented by t_s') but no signal, and rendering any filter function meaningless.

---

7 Cravatt, J.E. and Giles, M.K. (1990) An improved model of the TI deformable mirror device, *Proc. S.P.I.E.*, **1296**:110-124, *Advances in Optical Information Processing IV*, D.R. Pape (ed.).

8 Giles, M., Taylor, J., Grijalva, N. and Gioannini, B. (1987) Optical image correlation using a deformable mirror device: a feasibility study, *Proc. S.P.I.E.*, **753**:72-81, *Acousto-Optic, Electro-Optic and Magneto-Optic Devices and Applications*, S. Lucero (ed.).

9 Bock, B.D., Crow, T.A. and Giles, M.K. (1990) Design considerations for miniature optical correlation systems that use pixelated input and filter transducers, *Proc. S.P.I.E.*, **1347**:297-309, *Optical Information-Processing Systems and Architectures II*, B. Javidi (ed.).

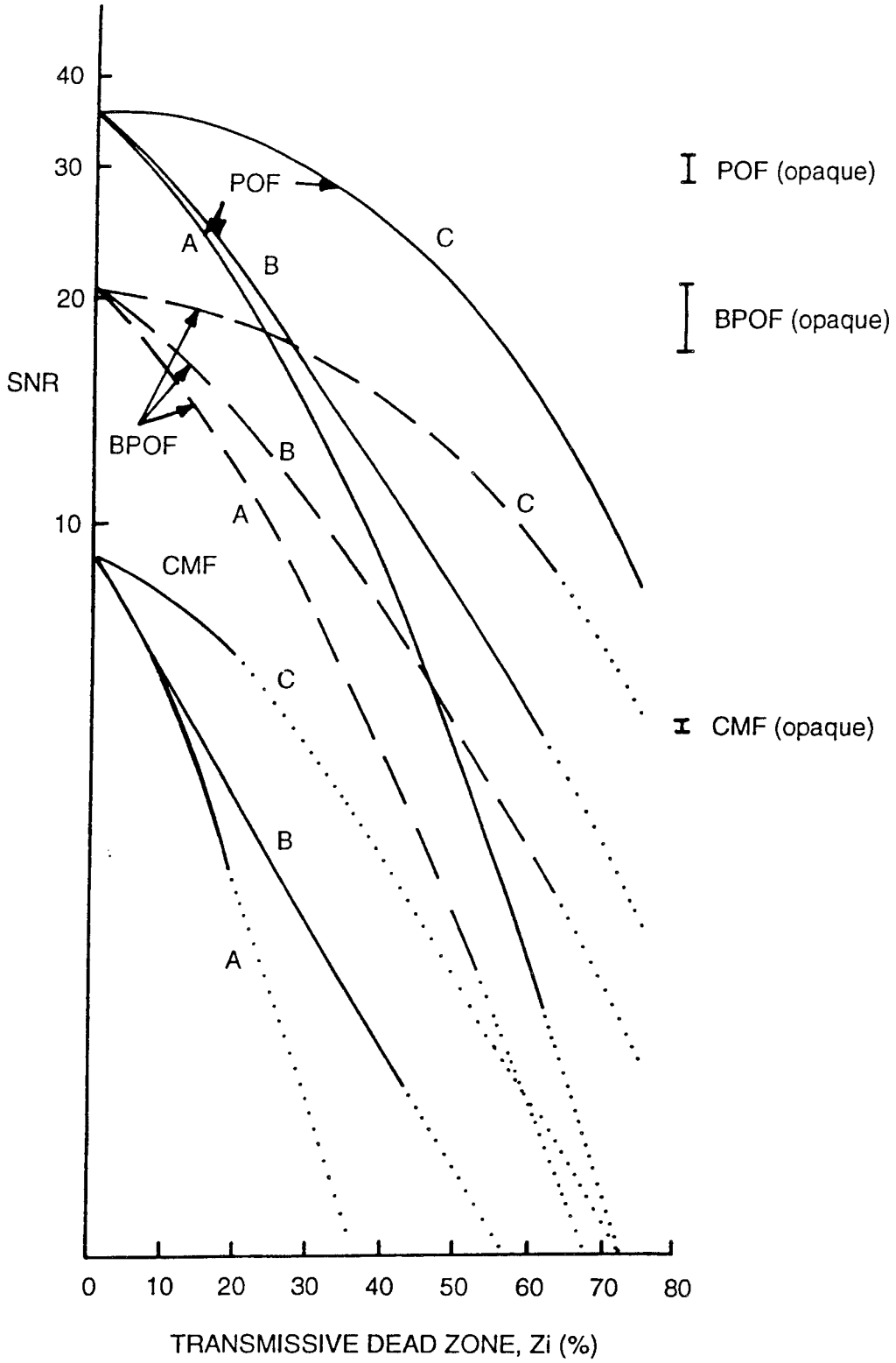

Figure 3. Normalized Correlation Peak Intensity I_p (Dashed Lines) Versus Transmissive Dead Zone Area (in Percent) for Case A With a 1-Pixel dc Block Inserted in the Filter Plane. The calculated values are indicated by black squares. The solid curves are for the corresponding opaque dead zone mode with no dc block included. The dotted curves give the normalized maximum intensities of those subsidiary peaks higher than I_p. Their calculated values are indicated by black circles.

The noise from the dead zones also enhances secondary peaks in the correlation pattern and for sufficiently large TDZs can even cause these secondary intensities to exceed the I_p. The intensity of the largest of these secondary peaks, given by I_{max}, is represented by a dotted curve in Figure 3 for each filter. Here, the dotted I_{max} curve for the CMF begins to rise above the I_p value at a TDZ ≈ 20 percent. The corresponding values for the BPOF and POF are approximately 65 percent and 75 percent, respectively. Beyond these values, the dotted curves rise very rapidly. At 100 percent TDZ we see from Eqs. (12)-(15) that k_T reduces to k_R only. Hence, the secondary peak is simply the maximum of the dc block-filtered image of the transparent input SLM, which in the present situation is 0.175.

Similar information for TDZ in the input plane only (Case B) is shown in Figure 4. The solid curves come from the Case B ODZ curves.[1] The dashed curves representing the TDZ I_p do not experience a minimum but monotonically decrease in magnitude with increasing TDZ.[10] For both of the phase filters the dashed curves stay fairly close to the solid curves up to DZs of about 50 percent. Since Z_2=0 in Case B, at 100 percent TDZ (Z_1=1), Eqs. (12)-(15) show that k_T reduces to k_{FR} only. Using the form of k_{FR} shown in Eq. (6), we see that k_{FR} is proportional to (constant * g) = (constant).G(0.0). Using Eq. (A-12) in the appendix this term eventually reduces to (constant).F^*(0, 0), where G(0, 0) and F^*(0, 0) are evaluated at $\xi_2=\eta_2=0$. Consequently, at 100 percent TDZ each filter produces its own characteristic I_p and I_{max}. Since the CMF pixels are attenuating, its I_p (and I_{max}) is the lowest of the three filters. On the other hand, the POF pixels do not attenuate so its I_p (and I_{max}) is the highest of the three. Although the BPOF pixels don't attenuate either, they divide the energy between a convolution and a correlation pattern so that its value of I_p (and I_{max}) is lower than that for the POF.

Similar information for TDZ in the filter plane only (Case C) is shown in Figure 5. The solid curves come from the Case C ODZ curves.[1] Just as in Case B the dashed curves decrease monotonically, only here they are much closer to the solid curves. This indicates that having TDZ only in the filter plane introduces less noise into the system than having TDZ only in the input plane, as in Cases A and B. In fact, for both of the phase filters the two curves stay fairly close together over the entire range. Since Z_1=0 in Case C, at 100 percent TDZ (Z_2=1) then $k_T=k_s$ only, which from the form shown in Eq. (4) is proportional to w'. Thus, the I_p and I_{max} are equal to the corresponding intensities on a dc block-filtered version of the signal image.

---

[10] Gianino, P.D., Horner, J.L. and Woods, C.L. (1990) Effects of SLM transmissive dead zones on optical correlation, *Proc. S.P.I.E.*, **1347**:240-246, *Optical Information-Processing Systems and Architectures II*, B. Javidi (ed.).

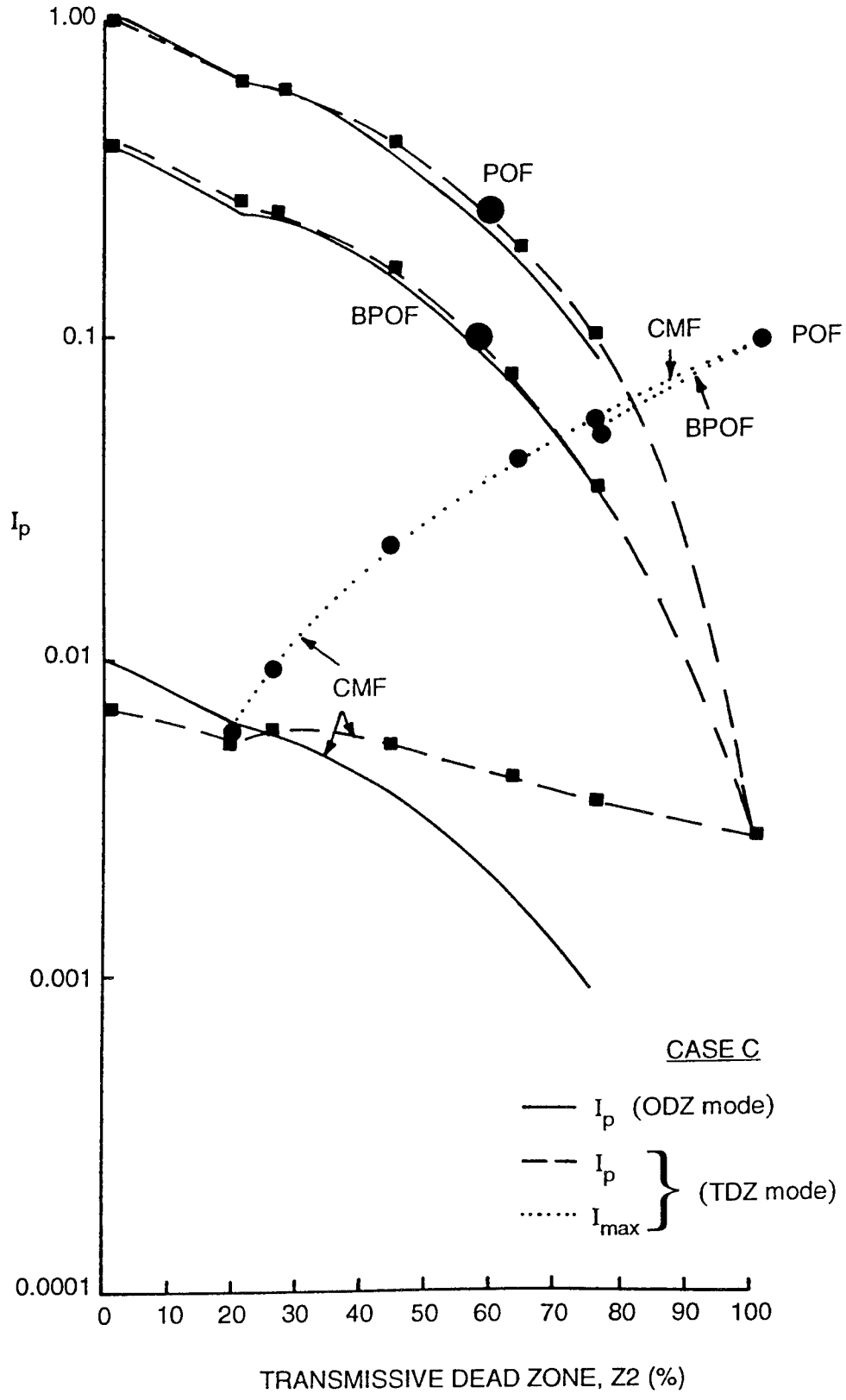

Figure 4. Same as Figure 3 Except for Case B.

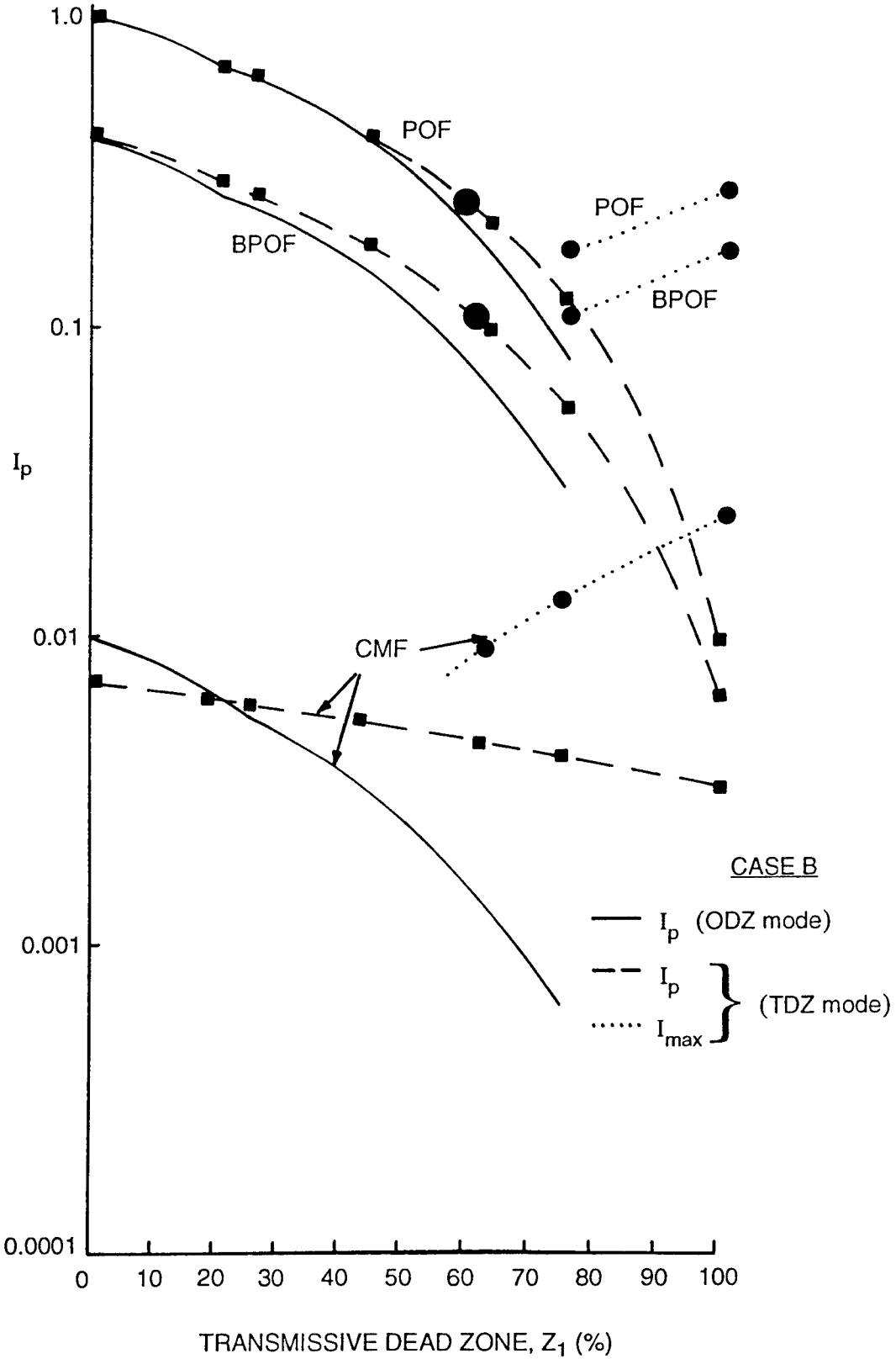

Figure 5. Same as Figure 3 Except for Case C.

As a performance guide for the two phase filters, we indicate those areas of TDZ that will cause I_p to decrease by 6 db (that is, by a factor of 4) below its zero dead zone value. These operating points are labelled by the large black dots in Figures 3, 4 and 5. This condition occurs at a TDZ value of approximately 39 percent for Case A (in which both SLMs have DZs) and at approximately 60 percent and 57 percent for Cases B and C, respectively (in which only one SLM has DZ). These values compare quite closely to those of 33 percent and 52 percent for Cases A and (B, C), respectively, under the ODZ condition with no dc block. The 6db condition cannot be designated for the CMF because its peaks are swamped by noise at small TDZ. These results clearly indicate the robust operation of the POF and BPOF while operating with TDZ noise.

4.2 Correlation Signal-To-Noise Ratio

The definition of the SNR is

$$SNR = (k_c)_{max} / \left\{ \sum_{j=1}^{n_T} (k_T)_j^2 \, (< 0.5\,(k_c)_{max}) / \, n_T \right\}^{1/2} . \qquad (16)$$

The numerator is the ODZ value and is identical in value to that in Eq. (1) of Reference 1. The denominator, however, includes the sum of all four k terms defined in Eqs. (12)-(15). The number of correlation points whose amplitudes $(k_T)_j$ are less than one-half of $(k_c)_{max}$ is given by n_T.

The SNR simulation results for the three cases utilizing the three filters in each case and a 1-pixel dc block in the filter plane are shown in Figure 6. Solid curves are used for the POF and CMF, while dashed curves are used for the BPOF. The dotted portions of these curves indicate that a secondary peak has become higher in amplitude than the correlation peak.[10] The vertical bars on the right hand side of Figure 6 indicate the range in variation in the SNR simulations using the three filters under the ODZ conditions when no dc block was used.[1]

The curves in Figure 6 show that SNR falls off significantly as TDZ increases. This is due to the increasing background noise. Such fall-off is in marked contrast to the relative flatness of the SNR plots when the DZ is opaque, as indicated by the vertical bars on the right side of the figure. For a fixed value of TDZ the POF is the best performing filter and the CMF is the worst. Also, performance is more adversely affected when the input has TDZ (as in Cases A and B) rather than the filter (as in Case C).[10] The substantial energy coming through input plane TDZ makes a large noise contribution while the signal is decreased. In fact, for input TDZ of about 8 percent the noise energy from the (64x64) pixel TDZ is equal to the energy in the (32x32) pixel input signal.

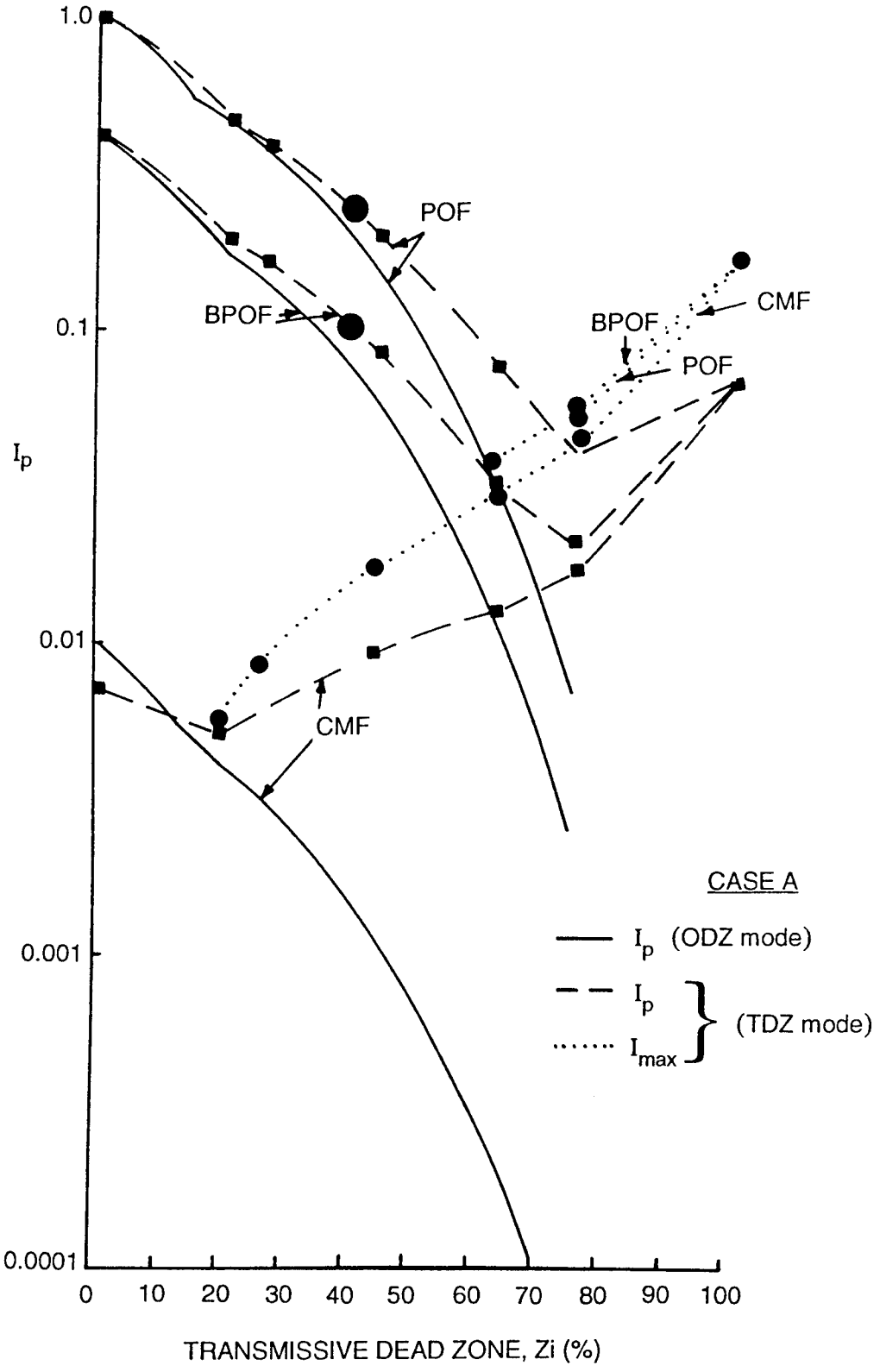

Figure 6. Correlation SNR Versus Transmissive Dead Zone Area (in Percent) Using Each of the Three Filters for Cases A, B and C. The dotted portions of each curve show when a subsidiary peak is higher in amplitude than the correlation peak. The vertical bars on the right indicate the SNR variations for each filter under opaque dead zone conditions and no dc block.

Table 2 demonstrates how the dc block removes a considerable portion of the background noise while slightly reducing the correlation peak. The net result is a significant increase in the SNR.[11] In the central portion of the table we list ratios of the SNR obtained with a 1-pixel dc block in the system to the SNR obtained with no block under representative conditions of TDZs. Inclusion of this dc block increases the SNRs typically by factors of 1.1 to 3.3. However, we note that the greatest effect occurs for Cases A and B, in which SLM1 contains TDZ, rather than for Case C, in which there is TDZ only in SLM2. The ratios in parentheses pertain to those conditions when a secondary peak is higher than the correlation peak. On the right side of Table 2 we list the ratios of correlation peak intensities under the same conditions as above, namely, with and without a dc block in the system. As expected, inclusion of a dc block diminishes I_p. However, these reduced peaks are still greater than the true correlation peaks given by k_c^2. We would also note that the dc block reduction of the TDZ background terms of Eqs. (13)-(15) is equivalent to the improvement in correlation SNR reported by Flannery, et al[11] and the reduction in clutter noise observed by Fielding and Horner.[12]

Table 2. Comparison of SNR and Peak Intensity for TDZ With and Without a 1-Pixel dc Block

		$(SNR)_{dcb}/(SNR)_{no\ dcb}$			$(I_p)_{dcb}/(I_p)_{no\ dcb}$		
Case	DZ (%)	POF	BPOF	CMF	POF	BPOF	CMF
A,B,C	0	1.2	1.1	1.7	0.97	0.99	0.72
A	25	2.3	2.2	(3.1)	0.82	1.00	(0.23)
B	44	2.1	1.6	3.3	0.75	0.94	0.17
C	44	1.3	1.2	(1.4)	0.96	1.02	(0.70)

Actually, the beam focused on the center of SLM2 has a half-power beamwidth of about 3 pixels. Consequently, a dc block that is 3 pixels square would significantly improve the SNR, even though it would lower I_p still further.

Similar information normalized to ODZ values (without a dc block) is supplied in Table 3. Apart from the values at 0 percent DZ we see that TDZ in <u>any</u> SLM, even with a dc block present, diminishes the SNR significantly compared to that for the ODZ condition. The right side of the table shows that TDZ enhances the peak intensities relative to the ODZ

---

[11] Flannery, D.L., Loomis, J.S. and Milkovich, M.E. (1988) Transform-ratio ternary phase-amplitude filter formulation for improved correlation discrimination, *Appl. Opt.*, **27**:4079-4083.

[12] Fielding, K.H. and Horner J.L. (1990) 1-f binary joint transform correlator, *Opt. Eng.*, **29**(9):1081-1087.

values by about 10 percent for the POF, by 10-30 percent for the BPOF, and by 40-80 percent for the CMF.

Table 3. Comparison of SNR and Peak Intensity for TDZ (With 1-Pixel dc Block) Relative to ODZ

		$(SNR)_{dcb}/(SNR)_{ODZ}$			$(I_p)_{dcb}/(I_p)_{ODZ}$		
Case	DZ (%)	POF	BPOF	CMF	POF	BPOF	CMF
A,B,C	0	1.2	1.1	1.7	0.97	0.99	0.72
A	25	0.57	0.47	(0.42)	1.12	1.22	(1.83)
B	44	0.33	0.31	0.31	1.15	1.26	1.72
C	44	0.82	0.75	(0.56)	1.06	1.10	(1.45)

4.3 Energy Throughput Efficiency

Table 4 shows what happens to the optical input energy at different locations in the system as TDZ varies. We show results only for the POF with a 1-pixel dc block in the filter plane for Cases A, B, and C. Values are stated in terms of percentages of the total light exiting from SLM1. The values in parentheses are the result when no dc block is present. The values in the last four columns refer to the following four quantities, respectively: light that SLM1 diffracts at too large an angle so that it misses the filter; light eliminated by the dc block; light that SLM2 diffracts at too large an angle so that it misses the detector; and light recorded by the detector. This latter value is the system's energy throughput efficiency and is also related to the peak-to-correlation energy (PCE).[13] With the exception of the light eliminated by the dc block, the other three partitions of energy are the TDZ counterparts of curves (2), (4), and (5) in Figure 8 of Reference 1. The values across any row always add to 100 percent. Note that Case C gives the highest throughput efficiencies.

[13] Kumar, B.V.K. and Hassebrook, L. (1990) Performance measures for correlation filters, *Appl. Opt.*, **29**:2997-3006.

Table 4. Energy Partitioning (Percent) Throughout Correlator With a POF and a 1-Pixel dc Block

(Values in parentheses are for no dc block)

	TDZ	% MISSING THE FILTER	% dc BLOCKED	% MISSING THE DETECTOR	% RECORDED BY DETECTOR
Case A	0	4.9	13.2	29.3	52.6
		(4.9)	(0)	(29.2)	(65.9)
	19	68.1	16.5	10.6	4.9
	25	64.4	19.5	11.4	4.7
		(64.4)	(0)	(12.6)	(23.0)
	44	50.0	28.8	15.0	6.1
	63	34.0	38.2	19.2	8.5
	75	23.0	44.6	21.4	11.0
	100	0.6	33.2	36.8	29.4
Case B	0	4.9	13.2	29.3	52.6
		(4.9)	(0)	(29.2)	(65.9)
	19	68.1	16.5	8.4	7.0
	25	64.4	19.5	9.5	6.5
	44	50.1	28.8	13.9	7.2
		(50.1)	(0)	(19.9)	(30.0)
	63	34.0	38.2	18.9	8.8
	75	23.0	44.6	22.3	10.1
	100	0.6	57.2	29.2	12.9
Case C	0	4.9	13.2	29.3	52.6
		(4.9)	(0)	(29.2)	(65.9)
	19	4.9	13.2	45.4	36.5
		(4.9)	(0)	(44.5)	(50.7)
	25	4.9	13.2	45.8	36.2
		(4.9)	(0)	(43.9)	(51.3)
	44	4.9	13.2	45.9	36.0
		(4.9)	(0)	(42.7)	(52.4)
	63	4.9	13.2	41.7	40.3
		(4.9)	(0)	(37.6)	(57.5)
	75	4.9	13.2	33.5	48.5
		(4.9)	(0)	(29.0)	(66.1)
	100	4.9	10.9	5.6	78.7

5. ANALYSIS OF CORRELATOR PERFORMANCE

The qualitative behavior of I_p and SNR with change in TDZ can be demonstrated from an analysis of Eqs. (12)-(15).

5.1 Peak Intensity

The total correlation output amplitude k_T is given by the sum of Eqs. (12)-(15) and the corresponding correlation intensity by $|k_T|^2$. Let us write this intensity as follows:

$$|k_T|^2 = |(1-Z_1)\,(1-Z_2)\,A_c + (1-Z_1)\,Z_2\,A_s + Z_1\,Z_2\,A_R + Z_1\,(1-Z_2)\,A_{FR}|^2, \tag{17}$$

where the A's represent the bracketed terms in Eqs. (12)-(15). The quantity A_R is independent of TDZ amount (as well as of the filter function) because it depends only on the q and r functions of Eqs. (8) and (10); whereas, the other three A quantities have a slight dependence on Z through the functions v and m of Eqs. (7) and (9). Nonetheless, to a first approximation, we can consider the A's to be constants with respect to Z.

We want to show, as demonstrated in Figures 3-5, that peak intensity should decrease as TDZ increases. As an example, consider Case C. Using Eq. (17) let us take the ratio of peak intensity I_p for arbitrary TDZ Z_2 to I_p at Z_2=0:

$$\frac{I_p(Z_2)}{I_p(0)} = \left|1 - \left(\frac{1 - A_s}{A_c}\right) Z_2\right|^2, \tag{18}$$

where the A's are computed at the location of the correlation peak. For input signals of the type used here and for the two phase filters, A_s is usually much less than A_c (at least over most of the range of Z). Consequently, we can see from Eq. (18) that as Z_2 increases, the above ratio diminishes, indicating that $I_p(Z_2)$ is getting progressively smaller than $I_p(0)$.

Similar arguments can be made for Cases A and B, thereby confirming the behavior of the two phase filter curves in Figures 3-5.

For the CMF the relative values of the A terms are sufficiently different from those of the phase filters to produce a minimum in the I_p-Z_i curves when the filter SLM contains TDZ. In Figures 3 and 5 we see that these minima occur in the vicinity of 20-25 percent DZ.

5.2 Signal-to-Noise Ratio

We can give an approximate analysis to show why the SNR curves behave as shown in Figure 6. Again, we take Case C as an example. Using the terms of Eq. (17) in the definition of SNR from Eq. (16) and dividing numerator and denominator by $(1-Z_2)$, we get for this case:

$$\text{SNR (Case C)} = \frac{(A_c)_p}{\left[\sum_j' \{A_c + [Z_2/(1-Z_2)]\, A_s\}_j^2\right]^{1/2} / \sqrt{n_T}} \tag{19}$$

where $(A_c)_p$ is the value of A_c at the location of the correlation peak and the prime indicates that the summation is to include only those points in the correlation pattern whose amplitudes are less than one-half of the correlation peak. Since the A_c and the A_s have only a weak dependence on the amount of DZ, as Z_2 increases, the denominator increases while the numerator remains relatively constant. Hence, regardless of the filter type, we can see from this expression that SNR diminishes with increase in TDZ.

A similar type of argument would hold for the SNRs in Cases A and B.

Figure 6 also shows that for each filter type the SNRs for the three cases are always in the order: SNR(Case C)>SNR(Case B)>SNR(Case A). We can show that this occurs upon considering the ratios of various SNRs. For example, if we take the ratio of SNR(Case C) to SNR(Case B), with both of them expressed in the form suggested by Eq. (19), we get, after cancellation of the common terms

$$\frac{\text{SNR (CASE C)}}{\text{SNR (CASE B)}} = \frac{\left[\sum_J' \{A_c + [Z_1/(1-Z_1)]\, A_{FR}\}_j^2\right]^{1/2}}{\left[\sum_J' \{A_c + [Z_2/(1-Z_2)]\, A_s\}_j^2\right]^{1/2}}. \tag{20}$$

Let us consider this ratio at some common TDZ so that $Z_1=Z_2$. Then, since A_{FR} is greater than A_s for the types of images used here, the numerator is always greater than the denominator. Consequently, SNR(Case C) is always greater than SNR(Case B) for any TDZ>0.

The same argument can be used to show that SNR(Case B) is always greater than SNR(Case A) for any TDZ>0.

5.3 Performance With a dc Block

Equation (A-20) in the Appendix shows that when a dc block is included, the value of each A term in Eq. (17) is diminished because a non-zero term has been subtracted from the original value. This means that when a dc block is included all of the A terms have smaller values than they would have without the block. When this information is inserted into the appropriate SNR equation, as shown, for example, in Eq. (19) for Case C, we can see that the denominator will decrease faster than the numerator. Consequently, the ratio will have a greater value than it would have had without the dc block.

6. DESIGNS FOR REDUCING FALSE PEAKS AND BACKGROUND

The presence of TDZ in the input plane introduces severe noise in the correlation pattern, resulting in false correlation peaks, additional background patterns and a SNR that depends on the correlator design. We now address each of these problems in turn.

6.1 Elimination of False Correlation Peaks

When the reference image used to produce the filter is the same size as SLM1 and this SLM contains TDZ, then false peaks are produced in the correlation. The matching of their edges contributes significantly to the overall pattern, as well as adding a large contribution to the correlation peak. As an example, we analyzed a Case B situation in which SLM1 had 44 percent TDZ, the POF in the filter plane was the same size as SLM1 and there was no dc block. Even with no signal in the input plane (s=0) a "correlation peak" was produced whose amplitude was just as large as that from a correlation between the POF and the regular input signal having no TDZ. Under these conditions, the total correlation amplitude would reduce to $k_T=k_{FR}$. We found that such false contributions to the correlation peak could be eliminated by mismatching the sizes of the reference image and the input SLM. We finally made the reference image one-half as large as the input SLM and positioned the image so that its edges (32x32 pixels) were well inside of the SLM1 edges (64x64 pixels).

6.2 Background Reduction

Since the BPOF correlation consists of two terms it is instructive to write its k_c term as $k_c=k_{c1}+k_{c2}$, where the subscript 1 refers to the correlation portion of k_c and the subscript 2 to the convolution portion. For the CMF and POF correlators, k_{c2} is zero.

If the centers of the input image and the filter reference image are located on the optic axis and both SLMs have TDZs, then all of the terms in Eqs. (12)-(15) (including k_{c1} and k_{c2} for a BPOF) will also have their centers on-axis in the correlation plane. Consequently, the three additional noise terms of Eqs. (13)-(15), plus the k_{c2} portion for a BPOF, will coherently add significant contributions onto and around the correlation peak. But, if the filter is fabricated from a filter reference image whose center has been diagonally offset from the optic axis, then the centers of k_{c1} and k_{c2} will move in opposite directions along this diagonal while the centers of k_s, k_R and k_{FR} will remain fixed on the optic axis. Moreover, if the input signal is translated, then the combination of k_{c1}, k_{c2} and k_s will translate as one fixed pattern. This process provides us with a means of separating the peak of k_{c1} from the background noise of k_{c2} and k_s. The same separation phenomenon was also observed in amplitude-encoded BPOFs.[14,15]

In our case, although the entire field in each plane extends to 128x128 pixels, the actual dimensions of the signal, the filter and the detector cover 64x64 pixels. The patterns of k_s, k_R, and k_{FR} cover 32x32, 64x64 and somewhat greater than 64x64 pixels, respectively. We shifted the filter reference image into a corner quadrant in the input plane by a distance of 32 pixels along the x and y directions. For the BPOF this reduced the backgrounds from Eqs. (12) and (13) since k_{c1} is shifted to a low intensity corner of both the k_s image and the k_{c2} convolution.

Additional noise reduction is provided by the dc block, which reduces the low frequency energy of the overlapping k_R and k_{FR} (as well as the $k_s$and k_{c2}) contributions. Consequently, both the shifting process and the dc block allow the peak to become relatively insensitive to the noise terms.

Downie and Reid[15] have reported that for their BPOF correlator, the correlation peak remained relatively independent of changes in threshold line angle. We studied the effects of changing the BPOF threshold line angle in Case A with Z_1=Z_2=44 percent and found a $\pm$17 percent maximum variation in SNR, as well as a $\pm$25 percent variation in I_p about the true correlation value. In Figure 3 this would mean that the value on the dashed curve at 44 percent TDZ could vary between $\pm$25 percent around the value on the solid curve. The I_p fluctuation came from coherent interference between the correlation peak and the background terms as their relative phases varied with threshold angle. The SNR fluctuation came from the phase variations of k_{c2} and k_{FR} as the change in threshold angle shifts the intensity distribution in the correlation plane relative to our 64x64 pixel detector. The substantial improvement in SNR (together with a decrease in I_p for a centered filter reference image) observed by Downie and Reid[15] results from the appearance and disappearance of a dc block in the amplitude-encoded BPOF as the threshold angle

---

[14] Flavin, M.A. and Horner, J.L. (1988) Amplitude encoded binary phase-only filters, *Proc. S.P.I.E.*, **938**:261-265, *Digital and Optical Shape Representation and Pattern Recognition*, R. Juday (ed.).

[15] Downie, J.D. and Reid, M.B. (1990) Mapping considerations for optimal binary correlation filters, *Appl. Opt.*, **29**:5235-5241.

changes.[16] Flannery, et al.,[17] have also reported similar variations for the BPOF correlation of objects in clutter.

A 3D correlation pattern for our system using a reference image mismatched to the SLM size, as well as off-axis shifts for the reference image and input signal, as described above, is shown in Figure 7. Here, the system has a BPOF, a 1-pixel dc block and no TDZ in SLM2 and a TDZ of 44 percent in SLM1 (Case B). The ridges surrounding the peak are due to the edges of the dc filtered k_{FR} term plus the correlation of the 64x64 pixel SLM1 edges with the 32x32 pixel reference image edges.

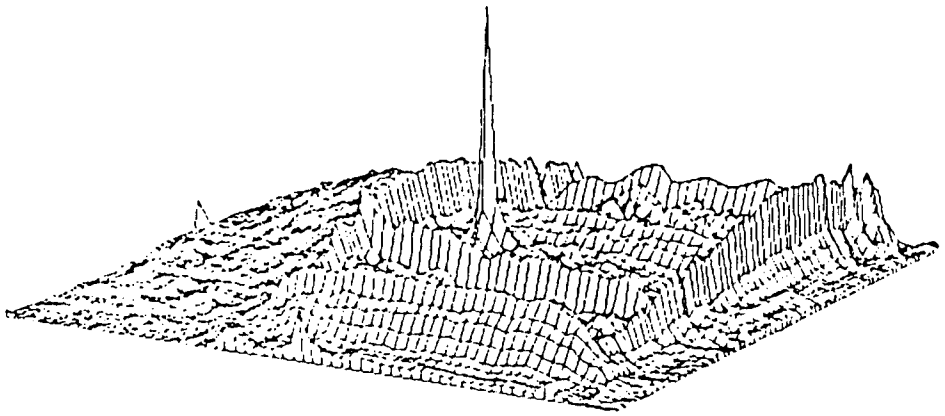

Figure 7. A Representative 3D Pattern for a Correlator Having a BPOF, a 1-pixel dc Block With No TDZ in SLM2 and a TDZ of 44 Percent in SLM1 (Case B). The reference image is one-half as large as, and is centered within, the input SLM. The SNR is 6.4.

6.3 Design-Dependent SNR

The quantitative value that one obtains for the SNR depends on how one chooses the spatial region over which the rms noise in the denominator is calculated. We have followed a standard convention of choosing a 64 square pixel input, filter and detector. In our design we chose the detector position by centering it on the correlation peak when the input image was centered in SLM1. With this design the peak will stay on the detector as long as the

---

[16] Khoury, J., Gianino, P.D., Kane, J. and Woods, C.L. (1994) Edge enhancement techniques for improving the performance of binary phase-only filter pattern recognition devices, *Opt. Eng.*, **33**(3):856-864.

[17] Flannery, D.L., Loomis, J.S. and Milkovich, M.E. (1988) Design elements of binary phase-only correlation filters, *Appl. Opt.*, **27**:4231-4235.

center of the input image is within SLM1. We use this detector area as the noise area for the rms calculation.

Our detector array contains most of the (0, 0) order of the correlation pattern, essentially all of the k_s image, (approximately 1/4 of k_{c2} for the BPOF) and roughly 1/2 of the k_R and k_{FR} terms. It also contains parts of the neighboring higher orders of the correlation pattern. The center portion of the area shown in Figure 7 corresponds to our detector, while the entire area is twice that of our detector. Furthermore, the reference image shift and input image position will determine what portions of the four k terms will fall within the detector. Clearly then, one can see that detector size affects the calculated value of SNR.

7. MIXED CASES OF TDZ AND ODZ

It is also possible to model mixed cases analytically, such as when one SLM contains transmissive dead zone (TDZ) only and the other opaque dead zone (ODZ) only or, when any one SLM contains both TDZ and ODZ. Consider, for example, the first situation in which the input SLM has ODZ of Z_1 and the filter SLM has TDZ of Z_2. We call this the (ODZ,TDZ) case. Here, $t_s(x_1, y_1) = t_s'(x_3, y_3) = 0$. So, from Eqs. (3)-(6) we see that only the k_c and k_s terms exist. Upon applying this information to Eq. (17) we can simplify that equation (referring to Table 1) to:

$$|k_T|^2(\text{ODZ, TDZ}) = (1 - Z_1)^2 |(1 - Z_2)\, A_c + Z_2 A_s|^2 = (1 - Z_1)^2 \bullet \left[|k_T|^2(\text{Case C})\right]. \tag{21}$$

Hence, the peak intensities for this situation can be obtained by multiplying the data in Figure 5 by the factor $(1\text{-}Z_1)^2$. Moreover, SNR for this situation is identically equal to the SNR(Case C) from Figure 6 because multiplication of k_T(Case C) by the constant value $(1\text{-}Z_1)$ does not affect the SNR.

In the reverse situation in which the input SLM has TDZ of Z_1 and the filter has ODZ of Z_2, which we call the (TDZ,ODZ) case, then $T_F(\xi_2, \eta_2) = t_F(x_3, y_3) = 0$. From Eqs. (3)-(6) we see that only the k_c and k_{FR} terms exist. Applying this information to Eq. (17) we can simplify that equation to

$$|k_T|^2(\text{TDZ, ODZ}) = (1 - Z_2)^2 |(1 - Z_1)\, A_c + Z_1 A_{FR}|^2 = (1 - Z_2)^2 \left[|k_T|^2(\text{Case B})\right]. \tag{22}$$

Consequently, the peak intensities for this situation can be calculated by multiplying the data in Figure 4 (Case B) by the factor $(1-Z_2)^2$ and the SNR is identically equal to SNR(Case B).

For the (ODZ,TDZ) case no dc block is necessary and no false correlation peaks due to edge correlation (see Section 4) occur; whereas, for the (TDZ,ODZ) case a dc block is necessary and contributions from edge correlation can occur. So, if one has a choice between these two combinations, it is generally better to place the ODZ SLM in the input plane.

The most general situation occurs when the DZ of any one SLM consists of both TDZ and ODZ, that is, $(DZ)_i=(TDZ)_i+(ODZ)_i$. In fact, all of the preceding analyses can be regarded as special cases of this situation, with either $(ODZ)_i$ or $(TDZ)_i$ equal to zero. This generalization can be very easily accounted for by considering Eqs. (12)-(15). There, the only terms that involve DZ directly are the Z_i and $(1-Z_i)$, which, of course, refer to $(TDZ)_i$ and $(AZ)_i$, respectively. So we see that the only portions of DZ that affect these equations are the amounts of TDZ and AZ; the opaque amount of DZ plays no role here at all. Hence, if in all of the previous equations we interpret all Z_i to refer to TDZ only and all $(1-Z_i)$ to refer to AZ only, then all of the previous equations will be applicable to this general case. Note that the k_c still represents the "true" correlation because it depends on the amounts of AZs only and is independent of the amounts of TDZ and/or ODZ that may be present.

8. CONCLUSIONS

Analytical results show that there are four basic terms making up the total correlation: one gives the true correlation, which is the same as that for the corresponding ODZ mode, and the other three form the background noise.

When the results from the mathematical analysis are combined with those from the computer simulation, we show that for a fixed value of TDZ:

1. Correlation performance in the form of SNR, peak intensity (I_p) and throughput efficiency is always the highest when a POF is used in the system, is slightly poorer for a BPOF, and is very poor for a CMF.

2. Insertion of a 1-pixel dc block at the center of the filter plane SLM enhances the SNR by removing the background in the correlation plane. The enhancement factors are from 2 to 3 when the TDZ is in the input SLM and about 1.5 when there is no DZ at all or when the TDZ is in the filter plane SLM only.

3. For either of the phase filters, I_p(Case B)>I_p (Case C) > I_p(Case A); whereas, for all three filters, SNR(Case C) > SNR(Case B) > SNR(Case A).

4. For either of the phase filters the I_p for the TDZ mode are always greater than those for the ODZ mode even when a 1-pixel dc block is used. This is not so for the CMF.

5. For an ODZ input and a TDZ filter the correlation is reduced from that of Case C by a factor of $(1-Z_1)^2$, but the SNR is the same as in Case C.

6. For a TDZ input and an ODZ filter the correlation is reduced from that of Case B by a factor of $(1-Z_2)^2$, but the SNR is the same as in Case B.

7. For an SLM containing both ODZ and TDZ the mathematical analysis derived here also holds, except that the term Z_i pertains only to the amount of TDZ in each pixel and the term $(1-Z_i)$ pertains only to the amount of AZ.

8. The efficiency of the signal light getting through to the detector is much greater for Case C than it is for Cases A or B.

As TDZ increases, the three salient results coming from the simulation are:

1. SNRs decrease by almost an order of magnitude. This is completely different from the ODZ mode in which the SNR was not affected at all by changes in ODZ area.

2. The correlation peak intensities I_p, although increased by TDZ noise, drop off by factors of 10 to 100, just as they did in the ODZ case. And these intensities vary slightly with changes in filter input position, as they did in the ODZ case.

3. For sufficiently large TDZ, secondary peaks in the correlation pattern become larger than I_p and keep increasing in amplitude up to 100 percent DZ. This is due to the large amount of light passing through the DZs. For Case A this occurs after approximately 60 percent DZ for both of the phase filters and after approximately 20 percent for the CMF.

One can always use the following as an approximate rule-of-thumb: I_p drops off by 6db (a factor of 4) below its zero DZ values when only one SLM has an active zone in the vicinity of 40 percent or when both SLMs have an active zone of 61 percent each.

9. RECOMMENDATIONS TO USERS

1. One should always try to place the SLM with the smaller amount of TDZ in the input plane.

2. When the input SLM has TDZ it is advantageous to insert a dc block in the filter plane.

3. For a square reference image it is absolutely necessary to mismatch the reference image and SLM sizes to minimize the false correlation enhancement from the matching of the input and TDZ edges.

4. To allow the correlation peak to become relatively insensitive to the TDZ (and possibly convolution) noise terms, one should fabricate the filter from a filter reference image whose center has been offset from the optic axis.

References

1. Gianino, P.D. and Woods, C.L. (1992) Effects of spatial light modulator opaque dead zones on optical correlation, *Appl. Opt.*, **31**:4025-4033.

2. Goodman, J.W. (1968) *Introduction to Fourier Optics*, McGraw-Hill Book Co., NY, Chap. 7, pp. 174-177.

3. Flavin, M.A. and Horner, J.L. (1989) Amplitude encoded phase-only filters, *Appl. Opt.*, **28**:1692-1696.

4. Yu, F.T.S., Cheng, F., Nagata, T. and Gregory, D.A. (1989) Effects of fringe binarization of multiobject joint transform correlation, *Appl. Opt.*, **28**:2988-2990.

5. Javidi, B. and Horner, J.L. (1989) Multifunction nonlinear signal processor: deconvolution and correlation, *Opt. Eng.*, **28**(8):837-843.

6. Davis, J.A., Merrill, E.A., Cottrell, D.M. and Bunch, R.M. (1990) Effects of sampling and binarization in the output of the joint Fourier transform correlator, *Opt. Eng.*, **29**(9):1094-1100.

7. Cravatt, J.E. and Giles, M.K. (1990) An improved model of the TI deformable mirror device, *Proc. S.P.I.E.*, **1296**:110-124, *Advances in Optical Information Processing IV*, D.R. Pape (ed.).

8. Giles, M., Taylor, J., Grijalva, N. and Gioannini, B. (1987) Optical image correlation using a deformable mirror device: a feasibility study, *Proc. S.P.I.E.*, **753**:72-81, *Acousto-Optic, Electro-Optic and Magneto-Optic Devices and Applications*, S. Lucero (ed.).

9. Bock, B.D., Crow, T.A. and Giles, M.K. (1990) Design considerations for miniature optical correlation systems that use pixelated input and filter transducers, *Proc. S.P.I.E.*, **1347**:297-309, *Optical Information-Processing Systems and Architectures II*, B. Javidi (ed.).

10. Gianino, P.D., Horner, J.L. and Woods, C.L. (1990) Effects of SLM transmissive dead zones on optical correlation, *Proc. S.P.I.E.*, **1347**:240-246, *Optical Information-Processing Systems and Architectures II*, B. Javidi (ed.).

11. Flannery, D.L., Loomis, J.S. and Milkovich, M.E. (1988) Transform-ratio ternary phase-amplitude filter formulation for improved correlation discrimination, *Appl. Opt.*, **27**:4079-4083.

12. Fielding, K.H. and Horner J.L. (1990) 1-f binary joint transform correlator, *Opt. Eng.*, **29**(9):1081-1087.

13. Kumar, B.V.K. and Hassebrook, L. (1990) Performance measures for correlation filters, *Appl. Opt.*, **29**:2997-3006.

14. Flavin, M.A. and Horner, J.L. (1988) Amplitude encoded binary phase-only filters, *Proc. S.P.I.E.*, **938**:261-265, *Digital and Optical Shape Representation and Pattern Recognition*, R. Juday (ed.).

15. Downie, J.D. and Reid, M.B. (1990) Mapping considerations for optimal binary correlation filters, *Appl. Opt.*, **29**:5235-5241.

16. Khoury, J., Gianino, P.D., Kane, J. and Woods, C.L. (1994) Edge enhancement techniques for improving the performance of binary phase-only filter pattern recognition devices, *Opt. Eng.*, **33**(3):856-864.

17. Flannery, D.L., Loomis, J.S. and Milkovich, M.E. (1988) Design elements of binary phase-only correlation filters, *Appl. Opt.*, **27**:4231-4235.

Appendix A

Derivation of Signals w', t_s', g, t_F and t_{dc}

A1. NO dc BLOCK IN FILTER PLANE

The signal amplitude $w(x_1, y_1)$ encoded on SLM1 due to the active areas in its pixels is given by:[6]

$$w(x_1, y_1) =$$

$$\left[\left\{ \sum_{n_x=-\infty}^{\infty} \sum_{n_y=-\infty}^{\infty} \delta(x_1 - n_x c_x)\, \delta(y_1 - n_y c_y)\, s(x_1, y_1) \right\} \odot (b_x v_x, b_y v_y) \right] . r_x r_y \qquad \text{(A-1)}$$

where s is the band-limited continuous signal that would produce digital samples. To model the finite size of the active area of the SLM pixels the sampled s is convolved with the 2D rect function $v_x v_y$ of Eq. (7). Then, this entire function is multiplied by the 2D rect function

$r_x r_y$ of Eq. (10), which accounts for the physical limits (L_x, L_y) of SLM1. This result is the same as Eq. (2) in Reference 1 except that the full 2D form is given and the last two terms indicate the SLM's physical limitation.

Before continuing with this analysis, we adopt the following notation for certain functions that occur often in the filter plane:

$$V_\xi \equiv \text{sinc}\,(b_x\,\xi_2) \equiv \text{FT}\,\{v_x\} \tag{A-2}$$

$$Q_\xi \equiv \text{rect}\,(c_x\,\xi_2) \equiv \text{FT}\,\{q_x\} \tag{A-3}$$

$$M_\xi \equiv \text{rect}\,(h_x\,L_x\,\xi_2/e_x) \equiv (e_x/h_x\,L_x)\,\text{FT}\,\{m_x\} \tag{A-4}$$

$$R_\xi \equiv L_x\,\text{sinc}\,(L_x\,\xi_2) \equiv \text{FT}\,\{r_x\} \tag{A-5}$$

where all of the quantities on the right side have already been defined and the Fourier transform (FT) equivalents are indicated. There will be another identical set, namely, V_η, Q_η, M_η, and R_η, in which the subscript x and variable ξ_2 are replaced by y and η_2, respectively. The additional terms h_xL_x and h_yL_y in the M functions of Eq. (A-4) come from the factors that scale space coordinates to spatial frequency coordinates (namely, $h_xL_x\xi_2 = x_2$ and $h_yL_y\eta_2 = y_2$).

The Fourier transform of w in Eq. (A-1) is represented by $W(\xi_2, \eta_2)$. We model SLM1 so that all orders of diffraction (indexed by the integers n_x, n_y) are discarded except the (0, 0) order because they fall outside of SLM2. The remaining transform is given as

$$W'(\xi_2, \eta_2) = (1 - Z_1)\left[\left(S(\xi_2, \eta_2) \cdot V_\xi V_\eta\right) \odot R_\xi R_\eta\right] \cdot Q_\xi Q_\eta. \tag{A-6}$$

where S is the Fourier transform of s and the Q terms account for the finite extent of SLM2, whose endpoints occur at $\xi_2 = \pm 1/2c_x$ and $\eta_2 = \pm 1/2c_y$. (When the $V_\xi V_\eta$ term is assumed to be flat, Eq. (A-6) gives the 2D form of Eq. (4) in Reference 1). Taking an inverse Fourier transform gives the amplitude function:

$$w'(x_3, y_3) = (1 - Z_1)\left[\left\{s(x_3, y_3) \odot v_x v_y\right\} \cdot r_x r_y\right] \odot q_x q_y. \tag{A-7}$$

The r terms show that w' is limited by the physical dimensions L_x, L_y of the detector.

As can be seen from Figure 1, the DZ in each pixel of SLM1 can be represented by the continuous function

$$D_1(x_1, y_1) = \text{rect}\left(\frac{x_1}{c_x}\right) \cdot \text{rect}\left(\frac{y_1}{c_y}\right) - b_x v_x \cdot b_y v_y. \tag{A-8}$$

Following the same reasoning as in Eq. (A-1) we obtain t_s, the signal emanating from SLM1 that comes solely from the TDZ, as

$$t_s(x_1, y_1) =$$

$$\left[\left\{\sum_{n_x=-\infty}^{\infty}\sum_{n_y=-\infty}^{\infty} \delta(x_1 - n_x c_x)\,\delta(y_1 - n_y c_y)\right\} \odot D_1(x_1, y_1)\right] \cdot r_x r_y \cdot \tag{A-9}$$

Its Fourier transform, T_s, can be shortened and modified to

$$T_s'(\xi_2, \eta_2) = Z_1 R_\xi R_\eta \cdot \mathcal{Q}_\xi \mathcal{Q}_\eta \cdot \tag{A-10}$$

in which all diffracted orders higher than (0, 0) are discarded because they miss the filter, and the physical dimensions of SLM2 are accounted for in the $\mathcal{Q}$ terms. Taking an inverse Fourier transform yields t_s', the amplitude in the output plane:

$$T_s'(\xi_2, \eta_2) = Z_1 R_\xi R_\eta \cdot \mathcal{Q}_\xi \mathcal{Q}_\eta \cdot \tag{A-11}$$

The amplitude of the filter transform function $G(\xi_2, \eta_2)$ encoded on SLM2 due to the active areas in the pixels is given by:

$$G(\xi_2, \eta_2) =$$

$$\left[\left\{ \sum_{n_x=-\infty}^{\infty} \sum_{n_y=-\infty}^{\infty} \delta(\xi_2 - n_x/L_x)\, \delta(\eta_2 - n_y/L_y)\, F^*(\xi_2, \eta_2) \right\} \odot M_\xi M_\eta \right] . \, Q_\xi Q_\eta \qquad \text{(A-12)}$$

where F^* is the band-limited continuous filter transform function for any one of the three desired filters and was originally derived from the signal w. The δ functions sample F^* at the center of each pixel at spatial frequency intervals of $1/L_x$, $1/L_y$. These intervals correspond to physical widths of h_x, h_y, respectively. To model the finite size of the active zone of the SLM pixels the sampled F^* is convolved with the 2D rect function $M_\xi M_\eta$ of Eq. (A-4). Then, this entire function is multiplied by the 2D rect function $Q_\xi Q_\eta$ of Eq. (A-3) which accounts for the physical limits of SLM2. Equation (A-12) is the 2D counterpart of Eq. (5) of Reference 1. Taking the inverse Fourier transform of Eq. (A-12) and keeping all diffraction orders for completeness, there results

$$g(x_3, y_3) =$$

$$(1 - Z_2) \left\{ \sum_{n_x=-\infty}^{\infty} \sum_{n_y=-\infty}^{\infty} f^*(-x_3 + n_x L_x - y_3 + n_y L_y) \, . \, m_x m_y \right\} \odot q_x q_y \qquad \text{(A-13)}$$

where $f^*(-x,-y)$ is the inverse Fourier transform of $F^*(\xi, \eta)$.

The DZ in each pixel of SLM2 can be represented by

$$D_2(x_2, y_2) = \text{rect}\left(\frac{x_2}{h_x}\right) . \, \text{rect}\left(\frac{y_2}{h_y}\right) - \text{rect}\left(\frac{x_2}{e_x}\right) . \, \text{rect}\left(\frac{y_2}{e_y}\right) . \qquad \text{(A-14)}$$

or, in spatial frequency coordinates,

$$D_2(\xi_2, \eta_2) = \text{rect}(L_x \xi_2) . \, \text{rect}(L_y \eta_2) - M_\xi M_\eta \, . \qquad \text{(A-15)}$$

The signal transmitted by the TDZs in SLM2 is given by

$$T_F(\xi_2, \eta_2) =$$

$$\left[\left\{ \sum_{n_x=-\infty}^{\infty} \sum_{n_y=-\infty}^{\infty} \delta(\xi_2 - n_x/L_x)\, \delta(\eta_2 - n_y/L_y) \right\} \odot D_2(\xi_2, \eta_2) \right] . \mathcal{Q}_\xi \mathcal{Q}_\eta . \tag{A-16}$$

Taking the inverse Fourier transform, evaluating the resulting convolution and separating the higher diffraction orders from the zero order, yields

$$t_F(x_3, y_3) = Z_2 q_x q_y - \sum'_{n_x} \sum'_{n_y} (1 - Z_2)\, \mathrm{sinc}\left(\frac{n_x e_x}{h_x}\right) . \mathrm{sinc}\left(\frac{n_y e_y}{h_y}\right) .$$

$$\frac{1}{c_x} \mathrm{sinc}\left(\frac{x_3 - n_x L_x}{c_x}\right) . \frac{1}{c_y} \mathrm{sinc}\left(\frac{y_3 - n_y L_y}{c_y}\right) \tag{A-17}$$

where the primes on the summations in the last term signify that n_x and n_y can go from $-\infty$ to $+\infty$, but cannot be zero simultaneously.

A2. WITH A dc BLOCK IN FILTER PLANE

If we insert a rectangular opaque dc block of p_x by p_y pixels at the center of SLM2 (with dimensions $p_x h_x$ by $p_y h_y$), its transmittance would be

$$T_{dc}(x_2, y_2) \equiv 1 - \mathrm{rect}\left(\frac{x_2}{p_x h_x}\right) . \mathrm{rect}\left(\frac{y_2}{p_y h_y}\right) . \tag{A-18}$$

This would scale in spatial frequency coordinates to

$$T_{dc}(\xi_2, \eta_2) = 1 - \mathrm{rect}\left(\frac{L_x \xi_2}{p_x}\right) . \mathrm{rect}\left(\frac{L_y \eta_2}{p_y}\right) , \tag{A-19}$$

which would transform to

$$t_{dc}(x_3, y_3) = \delta(x_3, y_3) - \frac{p_x p_y}{L_x L_y} \operatorname{sinc}\left(\frac{p_x x_3}{L_x}\right) \cdot \operatorname{sinc}\left(\frac{p_y y_3}{L_y}\right). \tag{A-20}$$

The signals G and T_F, given by Eqs. (A-12 and A-16), would have to be multiplied by $T_{dc}(\xi_2, \eta_2)$. This would result in rectangular sections being blocked out of their centers. The G function, for example, when modulated by this dc block, would transform as:

$$G(\xi_2, \eta_2) \bullet T_{dc}(\xi_2, \eta_2) \leftrightarrow g(x_3, y_3) \odot t_{dc}(x_3, y_3). \tag{A-21}$$

A similar expression would hold for T_F.

This dc block eliminates all the lower frequencies of light in the ranges

$$|\xi_2| \le p_x/2L_x \text{ and } |\eta_2| \le p_y/2L_y.$$

MISSION

OF

ROME LABORATORY

Rome Laboratory plans and executes an interdisciplinary program in research, development, test, and technology transition in support of Air Force Command, Control, Communications and Intelligence (C^3I) activities for all Air Force platforms. It also executes selected acquisition programs in several areas of expertise. Technical and engineering support within areas of competence is provided to ESD Program Offices (POs) and other ESD elements to perform effective acquisition of C^3I systems. In addition, Rome Laboratory's technology supports other AFSC Product Divisions, the Air Force user community, and other DOD and non-DOD agencies. Rome Laboratory maintains technical competence and research programs in areas including, but not limited to, communications, command and control, battle management, intelligence information processing, computational sciences and software producibility, wide area surveillance/sensors, signal processing, solid state sciences, photonics, electromagnetic technology, superconductivity, and electronic reliability/maintainability and testability.